Supplementary Information for:

A biosensor generated via high throughput screening quantifies cell edge Src dynamics

Akash Gulyani[1*], Eric Vitriol[1*], Richard Allen[1], Jianrong Wu[1], Dmitriy Gremyachinskiy[1], Steven Lewis[2], Brian Dewar[1], Lee M. Graves[1], Brian K. Kay[3], Brian Kuhlman[2], Tim Elston[1], and Klaus M. Hahn[1]

[1]Department of Pharmacology, University of North Carolina at Chapel Hill, 4009 Genetic Medicine, Campus Box 7365, Chapel Hill, NC 27599.

[2] Department of Biochemistry and Biophysics, University of North Carolina at Chapel Hill, 3010 Genetic Medicine, Campus Box 7260, Chapel Hill, NC 27599.

[3]Department of Biological Sciences, University of Illinois at Chicago, 845 West Taylor Street (MC 066) Chicago, IL 60607.

[*] These authors contributed equally to this work.

Address correspondence to Klaus M. Hahn[1] (email: khahn@med.unc.edu)

Supplementary Results

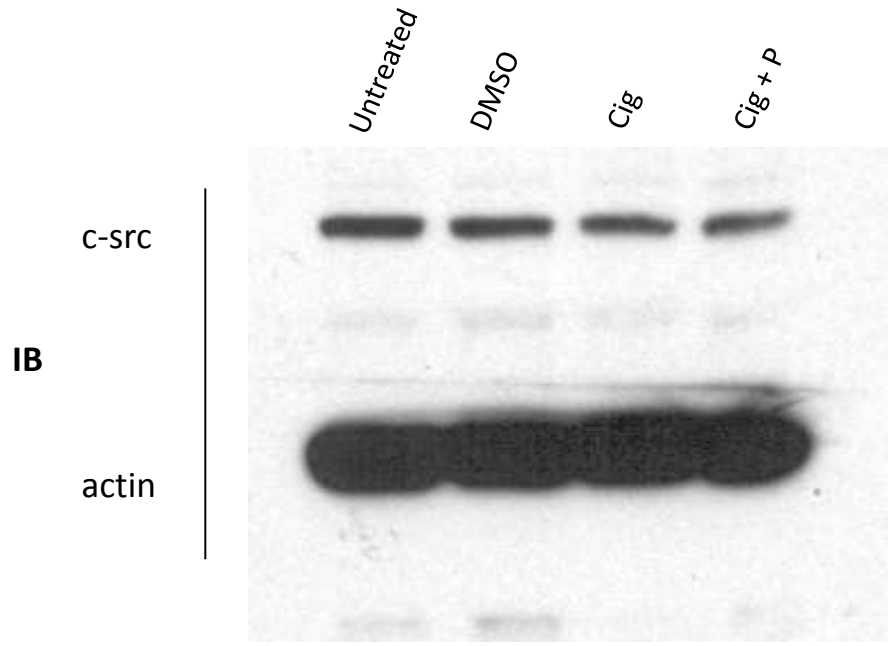

Supplementary Figure 1: Total Src levels do not change upon treatment of GN4 cell lysates. An immunoblot showing total Src levels in GN4 cell lysates, either untreated, treated with DMSO, treated with Ciglitazone (Cig) or treated with Ciglitazone after pre-treatment with pervanadate (global phosphatase inhibitor). Also shown are actin levels for all these conditions as a loading control. Also see previous papers describing detailed characterization of Src in GN4 lysates[1,2].

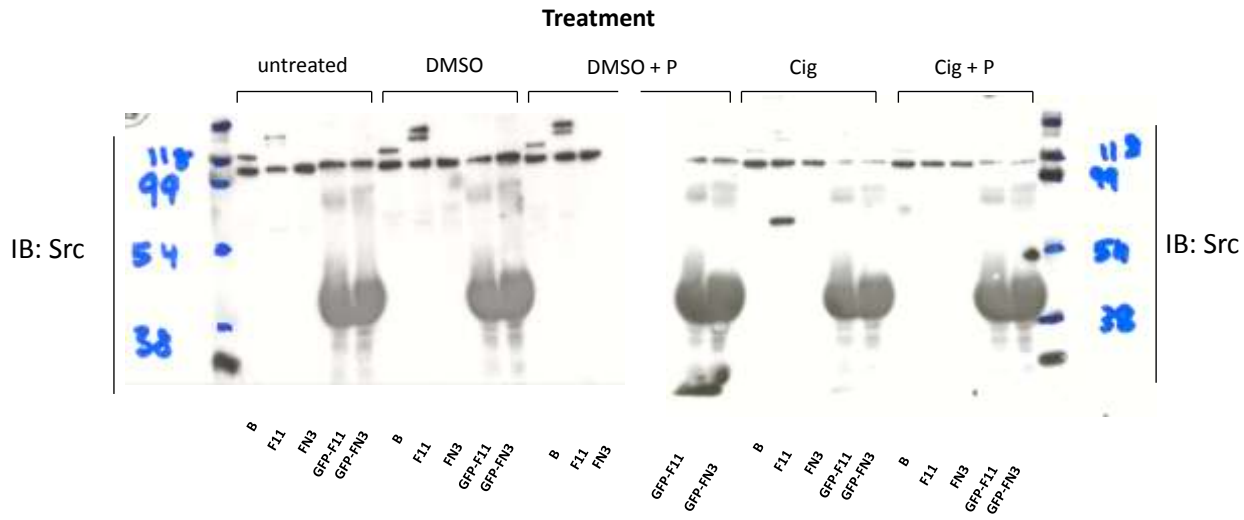

Supplementary Figure 2: **Immunoblot showing preferential binding of monobody 1F11 to active Src.** 1F11 monobody binding to Src in lysates from cells +/- the Src activator Ciglitazone. GN4 cells were either untreated, treated with vehicle DMSO, vehicle plus pervanadate pretreatment (P)**,** 50 µM Ciglitazone (Cig), or Ciglitazone with pervanadate pretreatment. Immunoblot (full blot shown here) was used to assay pulldown of Src by beads alone (B), the 1F11 monobody (1F11), control nonbinding monobody (wt FN3), GFP-1F11 with sub-optimal linker (G1F) or GFP-FN3 sub-optimal linker (GFN).

a

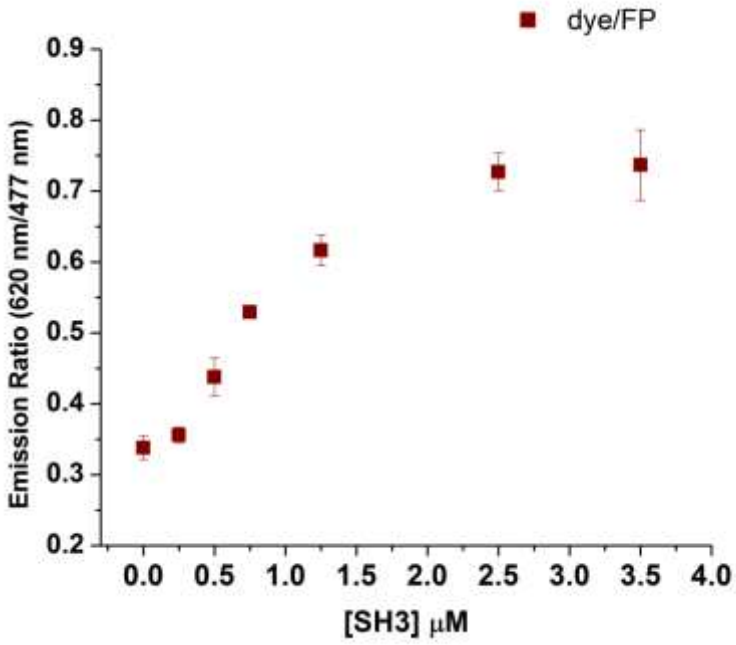

b

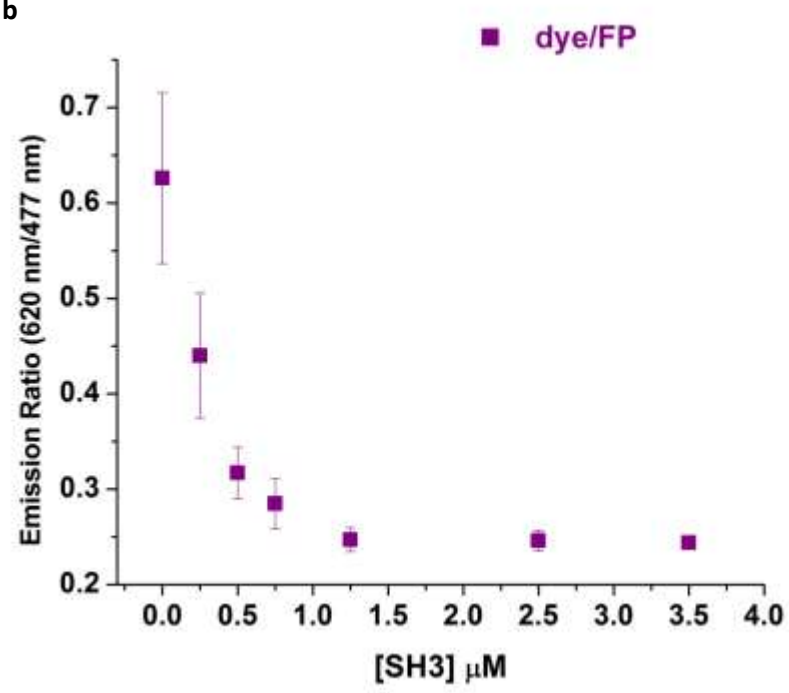

Supplementary Figure 3: **Response of additional biosensor versions to Src SH3**. Ratiometric (dye/m-cerulean) response of two biosensor versions, C53-mero87(**a**) and C52-mero53 (**b**) to c-Src SH3 in-vitro.

	Position 24, mero53	**Position 52, mero53**	**Position 53, mero87**
K_d (μM)	**0.69**	**0.26**	**0.97**
% Change in Ratio	51	61	114
Brightness (dye/m-cerulean FP)	1.6 – 2.4	0.6 – 0.2	0.3 – 0.7

Supplementary Table 1: Table showing data for three biosensor versions which showed responses suitable for use in living cells. The sensor in column 1 was chosen for live cell studies because of its brightness.

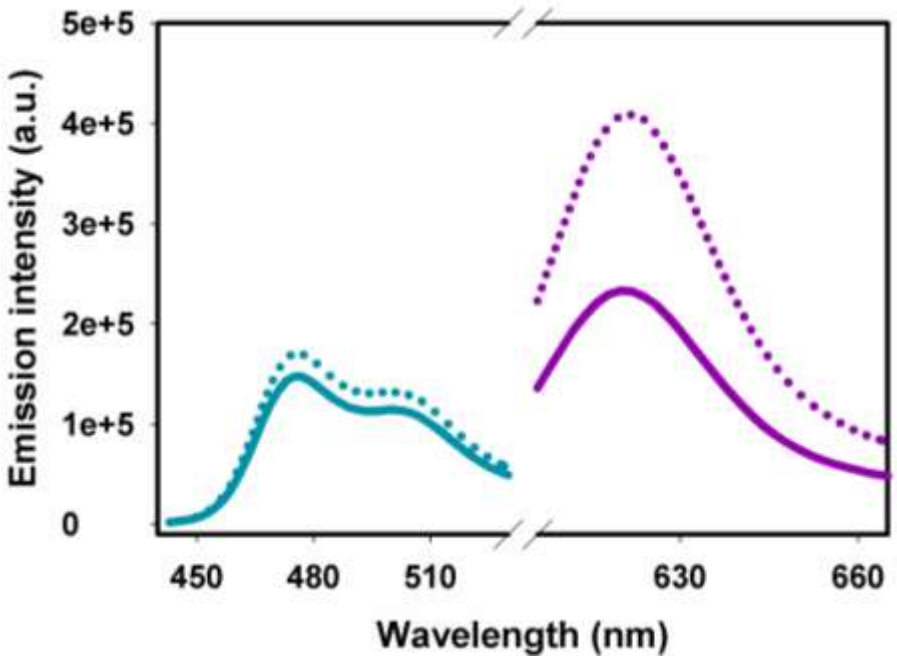

Supplementary Figure 4: Optimized merobody Src sensor suitable for live cell imaging. Mero53 and m-Cerulean emission spectra for 0.5 µM 1F11 merobody sensor alone (solid lines) or with saturating amounts (3.5 µM) of purified c-Src SH3 domain (dotted lines).

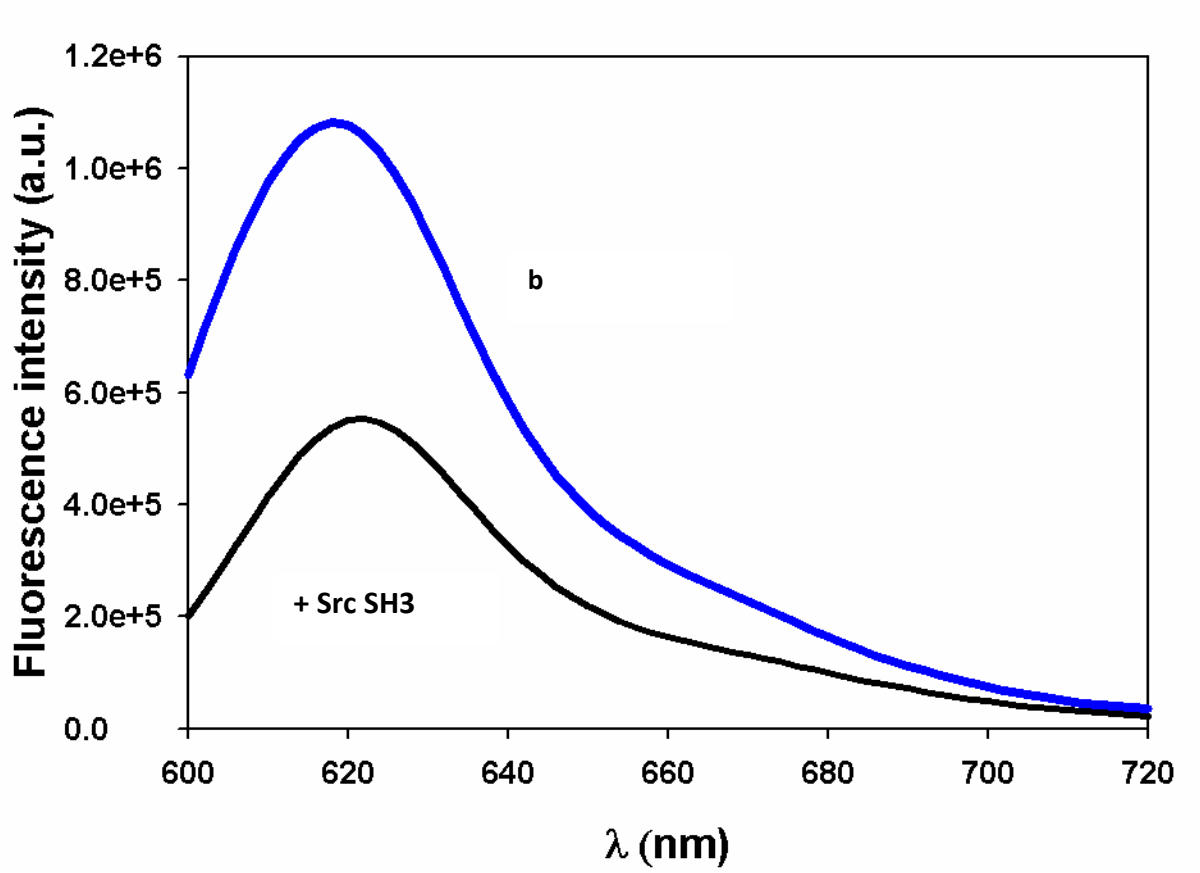

Supplementary Figure 5: Dye labeled 1F11 responds to SH3. Emission spectra showing increase in 1F11-mero87 (5 µM) fluorescence after addition of c-Src SH3 (22 µM). A 1F11 mutant with cysteine insertion at residue 53 was used for dye labeling; λ_{Ex}= 596 nm. Although this 1F11-mero87 does show response to c-Src SH3 in-vitro, it is unsuitable for live cell imaging due to uneven, punctate distribution in live cells (see Supplementary Figure 6).

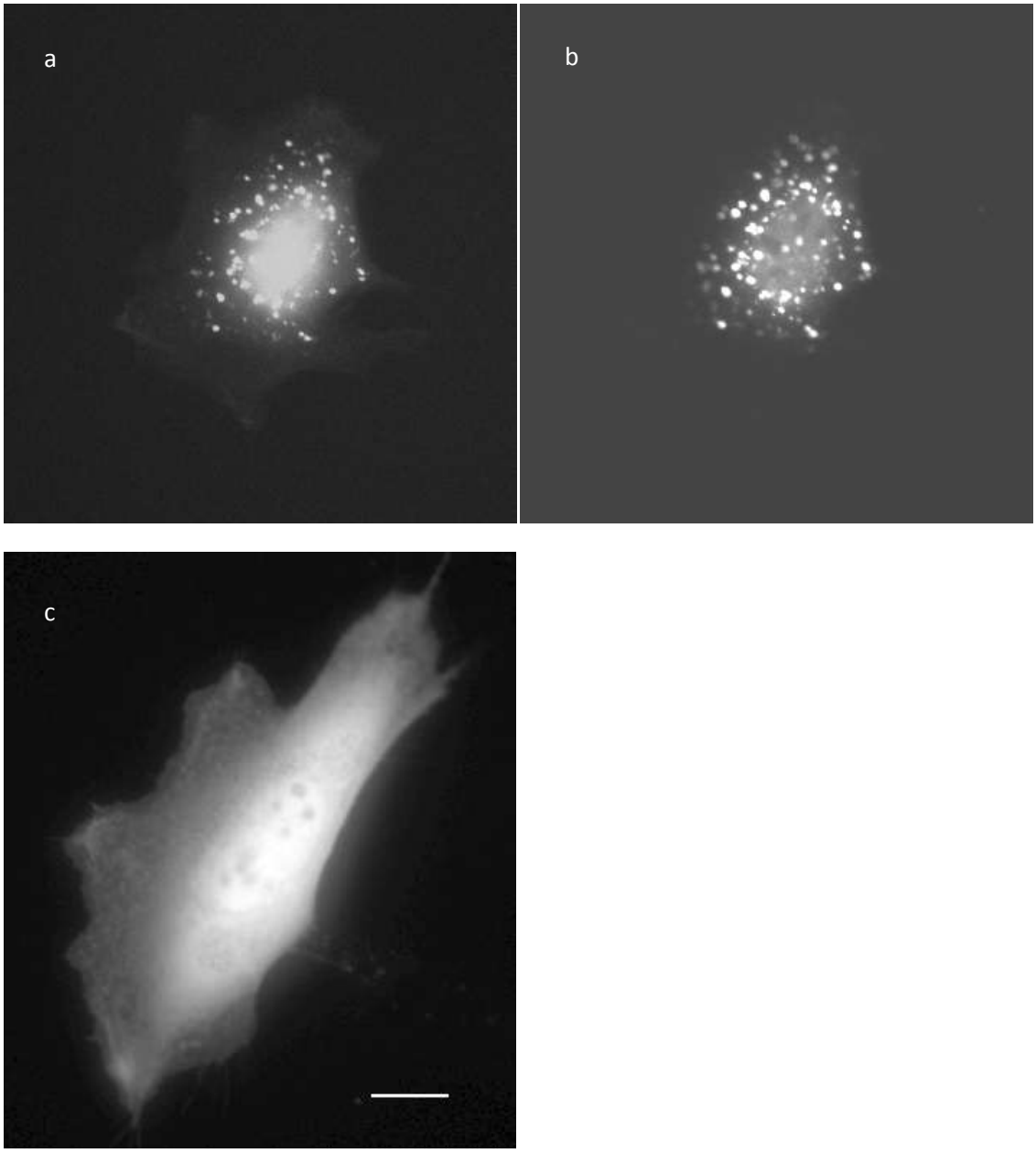

Supplementary Figure 6: Distribution of 1F11 conjugates in mouse embryo fibroblasts before and after optimization of fluorescent protein attachment . Fluorescent micrographs of un-optimized Alexa 488 (a) or mero87 (b) labeled single-cysteine 1F11 monobody microinjected in mouse embryo fibroblasts (MEF) cells show punctate, non-uniform districation. In contrast, final 'merobody' biosensor (c) is uniformly distributed (scale bar 10 µm, nonlinear scaling used to clearly show both cell edges and perinuclear region)

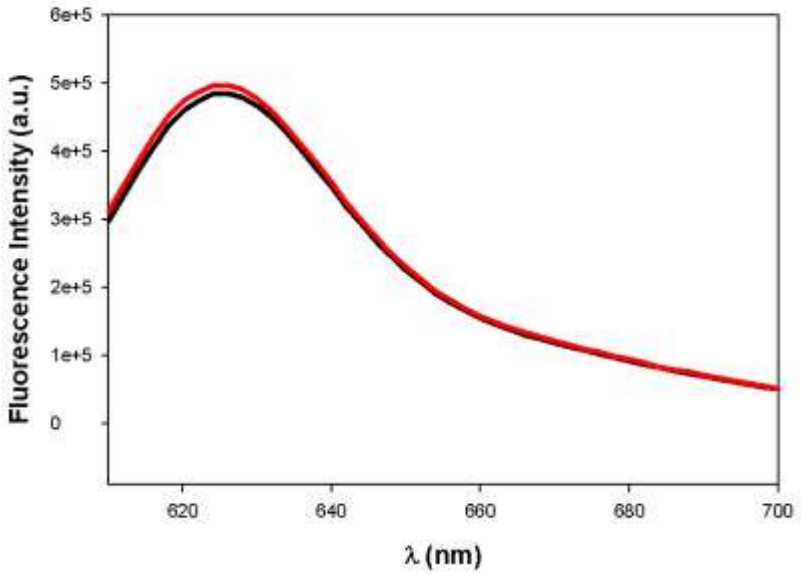

Supplementary Figure 7: Dye labeled GFP-1F11 with short, sub-optimal linker does not respond to c-Src SH3. Emission spectra showing no change in the dye emission for GFP-1F11-mero87 (5 µM)(short linker) after addition of c-Src SH3 (25 µM). 1F11 mutant with cysteine insertion at residue 53 was used for fusion and dye labeling; λ_{Ex}=596 nm.

MAHHHHHHGS VSKGEELFTG VVPILVELDG DVNGHKFSVS GEGEGDATYG KLTLKFISTT
GKLPVPWPTL VTTLTWGVQC FARYPDHMKQ HDFFKSAMPE GYVQERTIFF KDDGNYKTRA
EVKFEGDTLV NRIELKGIDF KEDGNILGHK LEYNAISDNV YITADKQKNG IKANFKIRHN
IEDGSVQLAD HYQQNTPIGD GPVLLPDNHY LSTQSKLSKD PNEKRDHMVL LEFVTAAGIT
LGMDELYKGS GSGSTSGSGK PGSGEGSTKG SVSDVPRKLE VVAATPTSLL ISWDAPGISQ
GYYRITYGET GGNSPVQEFT VPGSKSTATI SGLKPGVDYT ITVYAYSRPL PSKPISINYR
T

Supplementary Figure 8: Design of the biosensor for ratiometric imaging (FP m-Cerulean linked to the Src binder 1F11). The amino acid sequence of the biosensor construct with FP in cyan and FN3 binder (1F11) in blue. The flexible linker region, adapted from linkers used earlier (2,3), is shown in bold black. In red is the alanine residue in 1F11 that was mutated to cysteine for dye labeling in the final merobody Src family sensor (see main text). In purple is the proline residue (P80) that was mutated to alanine in non-binding control. In orange are other residues screened for dye placement and optimization.

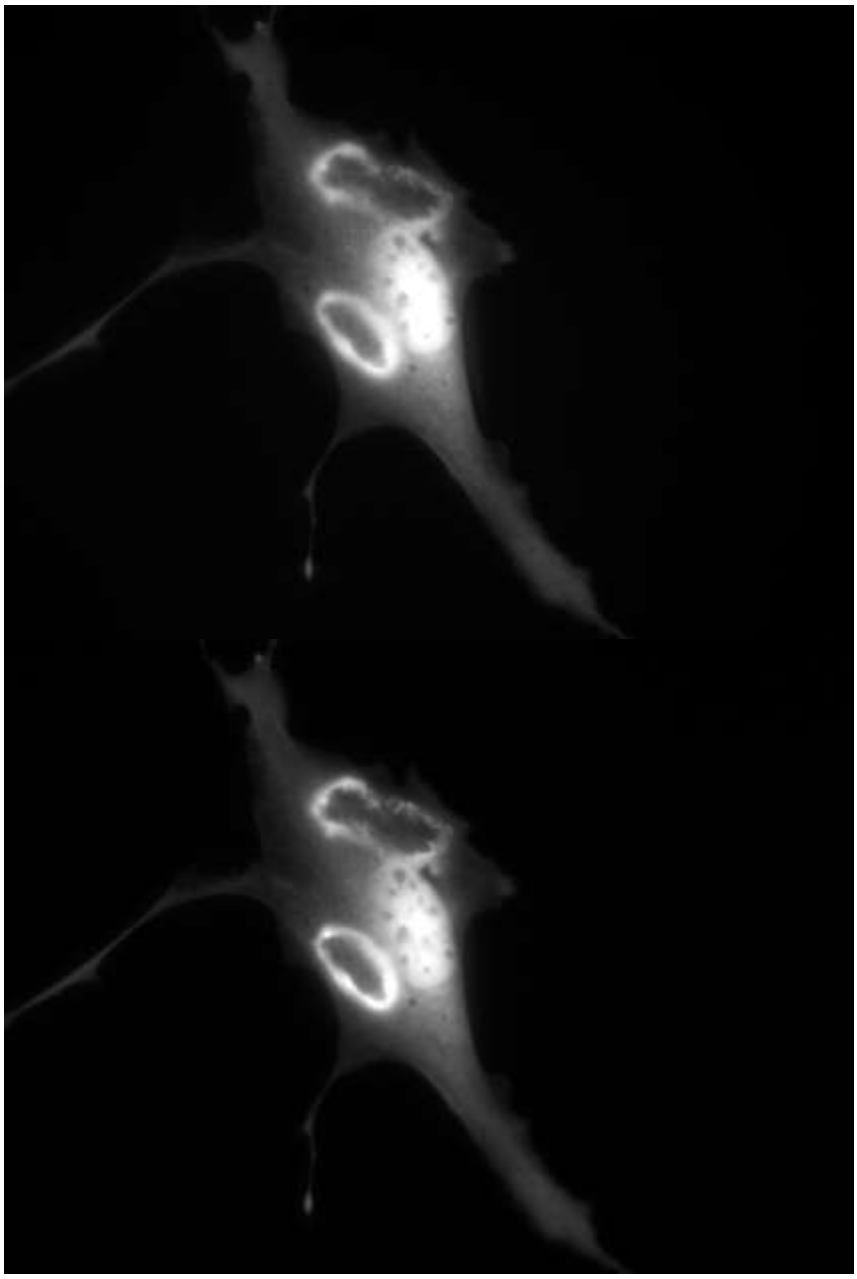

Supplementary Figure 9: Merobody sensor in ruffles. Example images of the m-Cerulean (top) and the dye Mero53 (bottom) channels used to generate the ratio image in **Fig. 4a** of the main text.

a

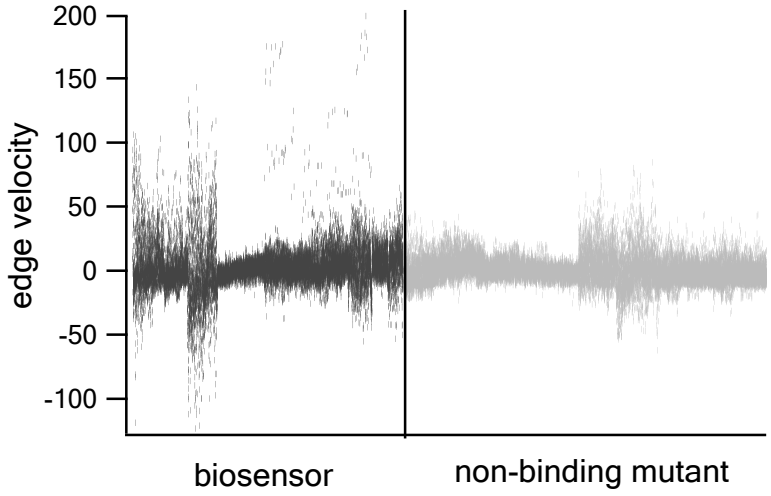

b

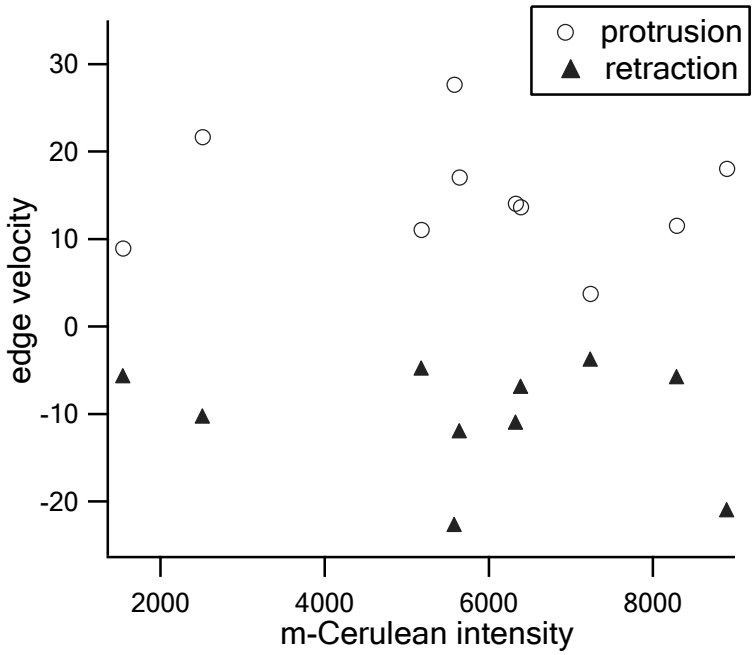

Supplementary Figure 10: Merobody SFK sensor does not perturb cell protrusion dynamics. a) Distribution of cell edge velocities (pixels/second x 10) of Ptk1 cells with biosensor or non-binding control. Negative velocity indicates cell retraction. **b)** Ptk1 cell edge velocity as a function of merobody sensor concentration (CFP intensity /area) in cells. Edge velocity shows no correlation with the amount of biosensor injected.

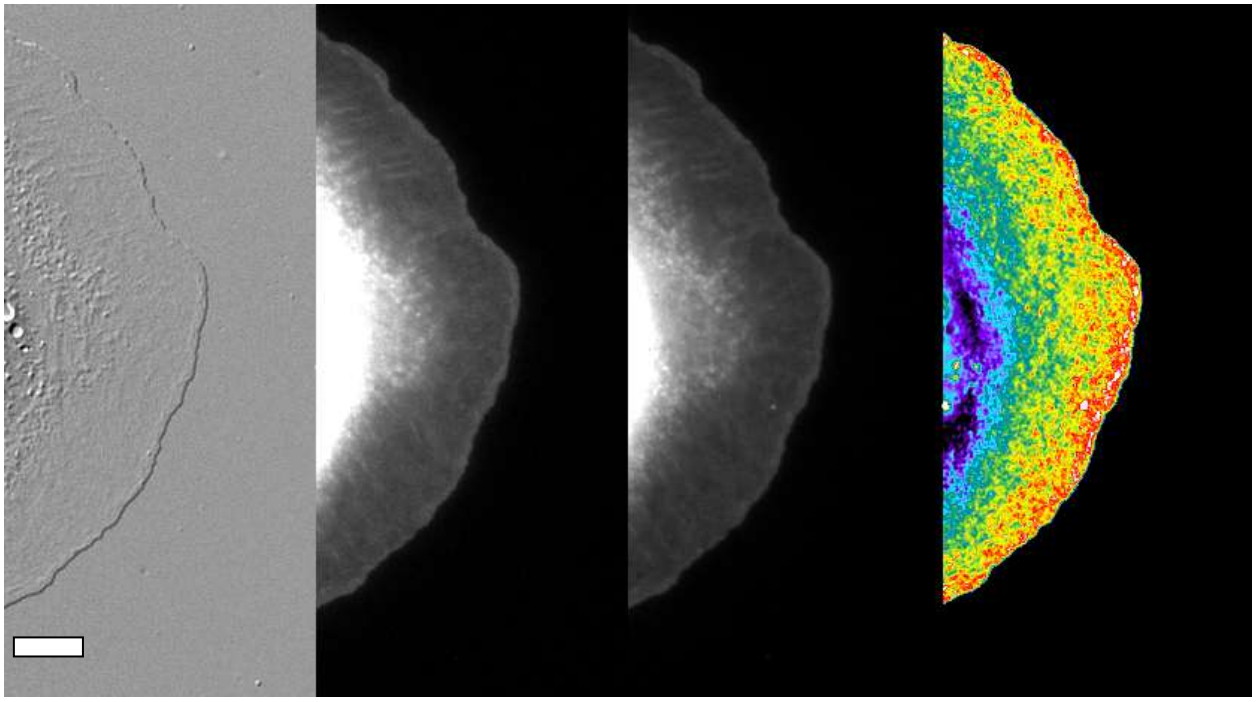

Supplementary Figure 11: Merobody sensor at the cell edge. Example images of (from the left) DIC, m-Cerulean, dye Mero53 and dye/FP ratio channels. The m-Cerulean and dye channels were used to generate the ratio image at right. Scale bar = 10 μM.

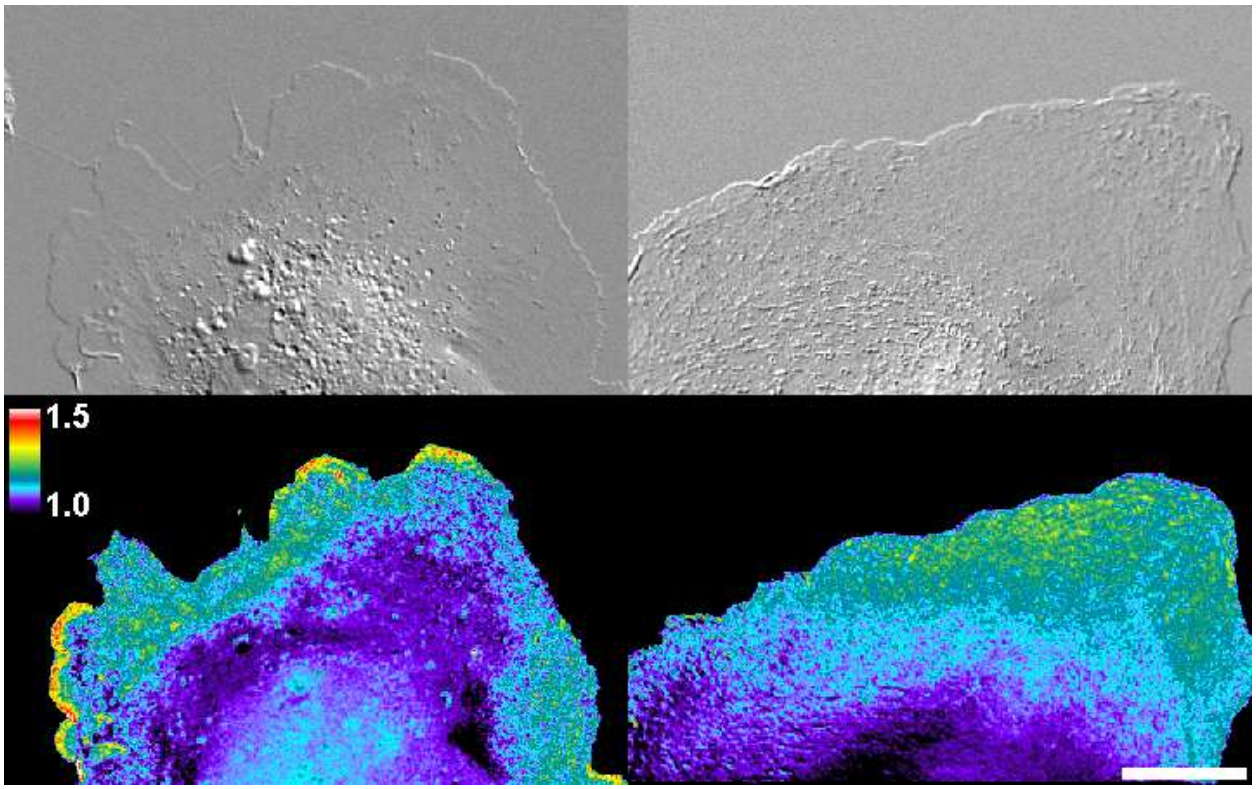

Supplementary Figure 12: SFK merobody biosensor and control in cell protrusions. DIC (top) and fluorescence ratio (bottom) images of the merobody bio sensor (left panels) and the non-binding control (right panels). Quantitation and statistical analysis using automated edge tracking and line scan analysis have also been carried out to compare ratio changes shown by the biosensor and the non-binding control (main text **Fig.5**)

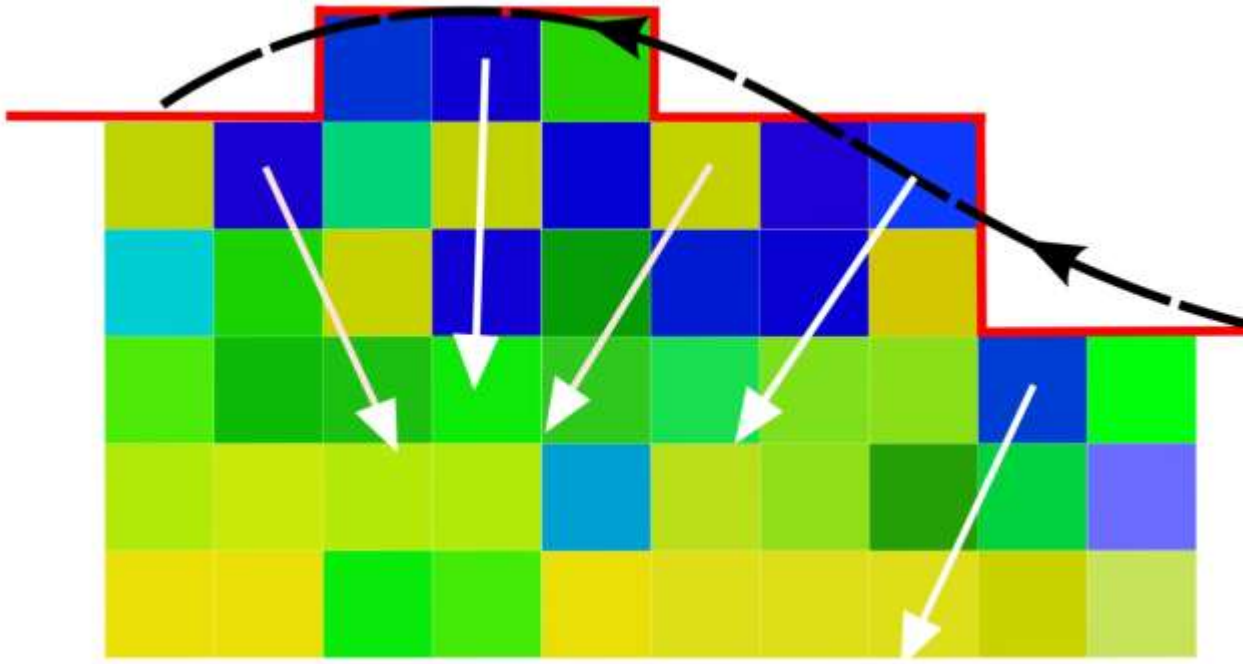

Supplementary Figure 13: Automated line scanning of Src activation dynamics in constitutive protrusions and retraction. Linescans (white arrows) are taken from every pixel at the cell edge (red line) in a direction normal to a smoothed edge (dashed line). Ratio intensity values at a given point along the linescan are bi-linearly interpolated from the four pixels surrounding that point.

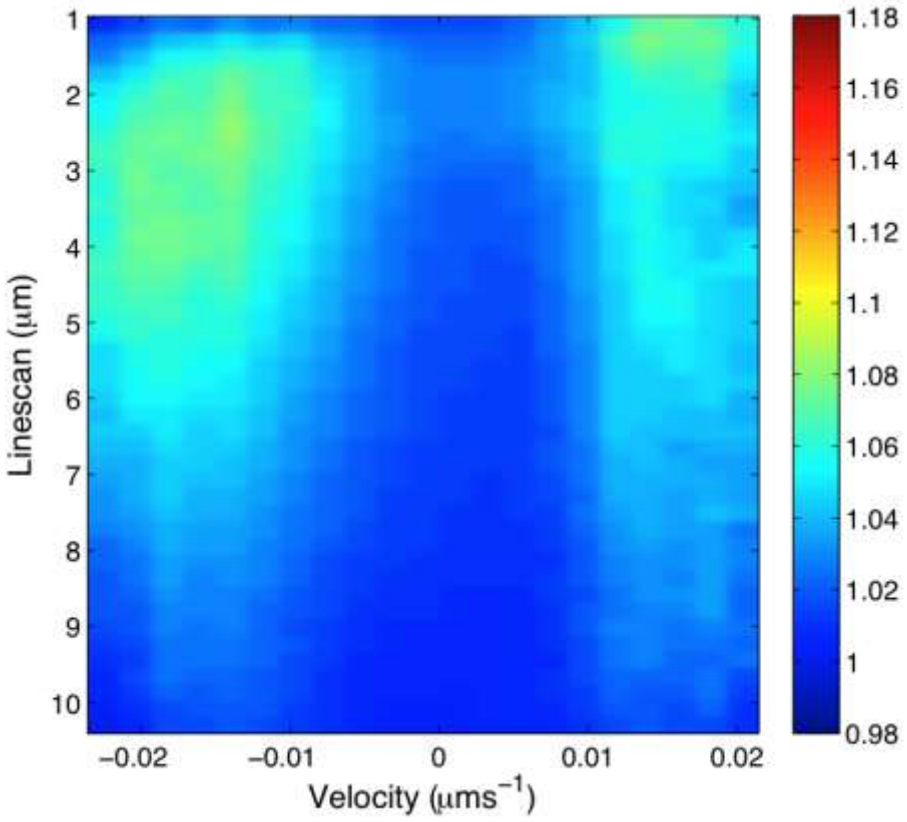

Supplementary Figure 14: PP2 treatment attenuates Src activation. Automated line scans analysis showing PP2 treatment reducing or abolishing Src activation as reported by the merobody Src sensor. Shown here is the response of the merobody biosensor after (>200 secs) treatment with the Src inhibitor PP2. In comparison with Figure 5 (main text) treatment of PP2 has inhibited the biosensor.

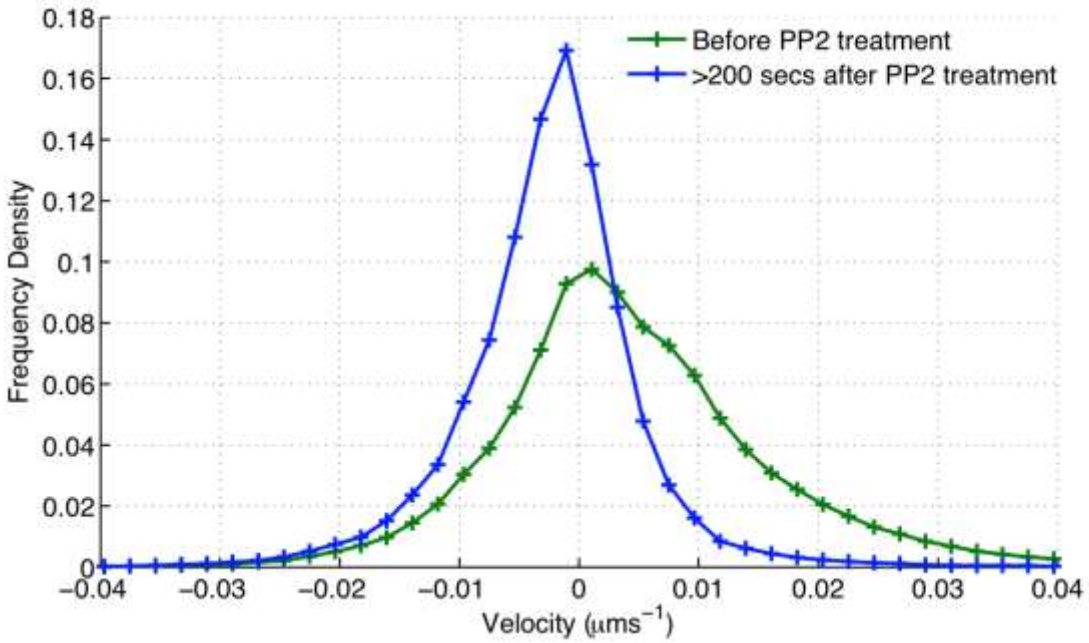

Supplementary Figure 15. Inhibition of Src activity effects protrusions dynamics. Histograms of the velocity of cell edges before and after (>200 secs) treatment with the Src inhibitor PP2.

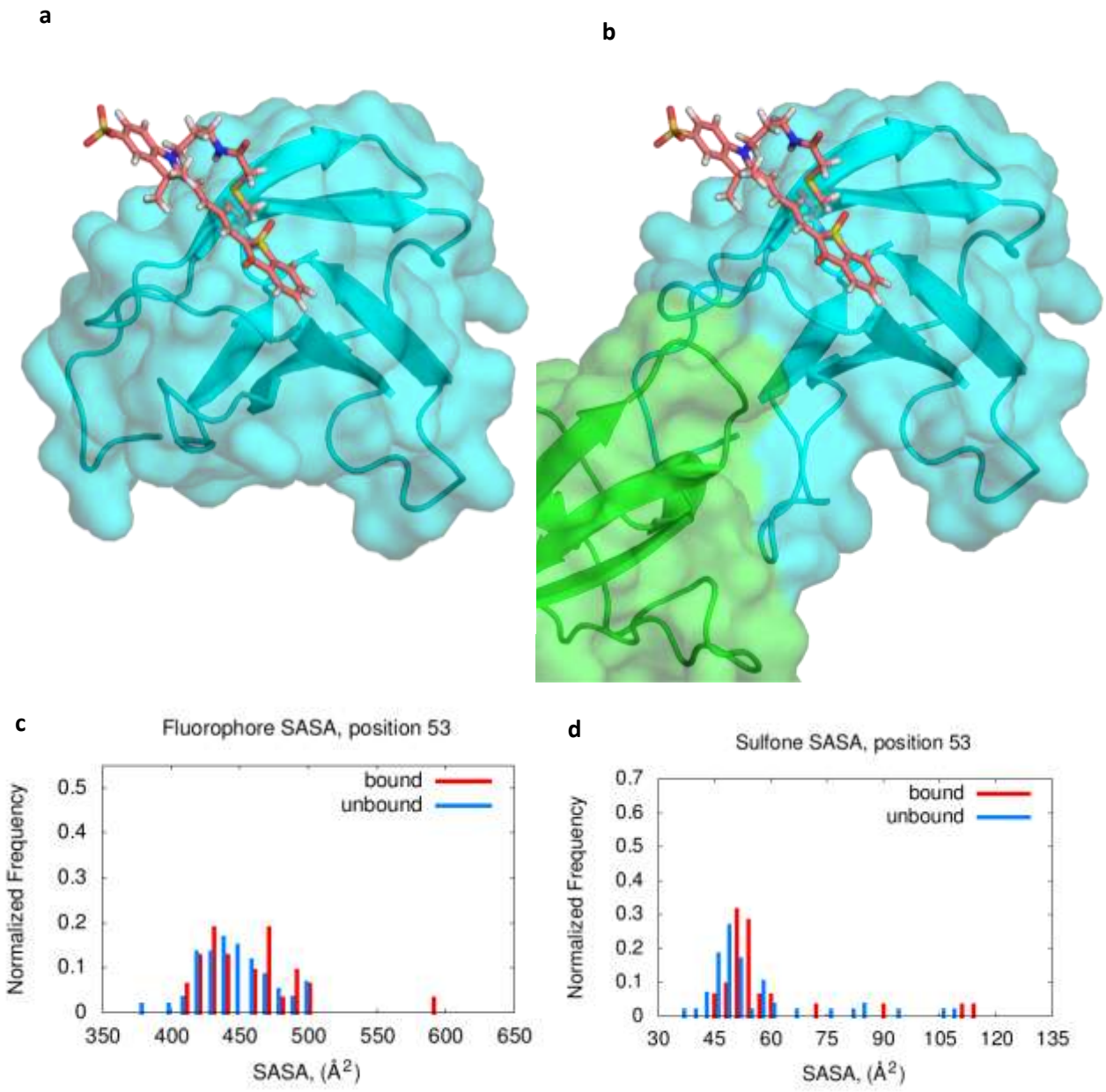

Supplementary Figure16. Solvent accessibility of mero53 is not significantly altered when the dye is attached at the 'unresponsive' position 53 on the merobody scaffold. Shown here (**a,** unbound**; b,** bound) are models of the 1F11-dye/cSrc-SH3 complex, with the dye at position 53. cSrc-SH3 is in green, 1F11 in blue, and the dye in salmon. In both cases the highest-scoring models found are shown. Also shown are the solvent accessible surface area (SASA) distributions for the fluorophore (**c**) and the sulfone group (**d**) for the top 0.5% of the models with dye mero53 at position 53.

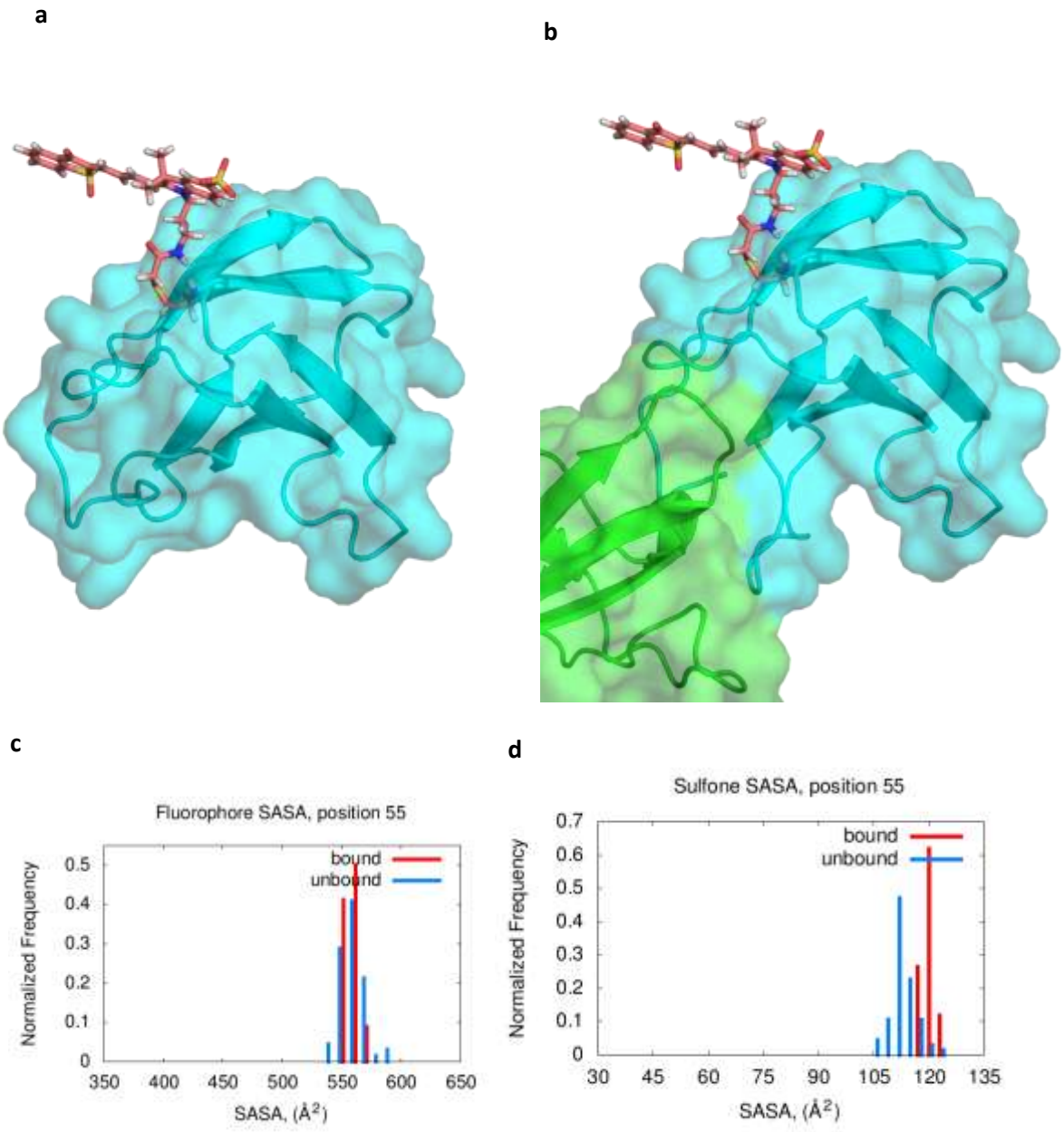

Supplementary Figure 17. Solvent accessibility of mero53 is not significantly altered when the dye is attached at the 'unresponsive' position 55 on the merobody scaffold. Shown here (**a,** unbound**; b,** bound) are models of the 1F11-dye/cSrc-SH3 complex, with the dye at position 55. cSrc-SH3 is in green, 1F11 in blue, and the dye in salmon. In both cases the highest-scoring models found are shown. Also shown are the solvent accessible surface area (SASA) distributions for the fluorophore (**c**) and the sulfone group (**d**) for the dye meo53 at position 55. The top 0.5% of the models by score are shown.

Supplementary videos:

Supplementary video 1: **Src activation in fibroblasts with PDGF stimulation**. Live cell imaging of NIH 3T3 fibroblasts microinjected with Src family merobody sensor after PDGF stimulation. Left panel shows movie of DIC images while the right panel shows time-lapse of ratio images (dye/FP). Magnification 40X; 2x2 binning. Movie acquired with 10 s interval. Time stamp on video indicates elapsed time; color bar indicates magnitude of ratio change. Src activation is seen at the cell edges and in dorsal linear and circular ruffles.

Supplementary video 2: **Src activation at the cell edge in PDGF stimulated fibroblasts**. Live cell imaging of the cell edge of a PDGF stimulated NIH 3T3 fibroblast microinjected with Src family merobody. Left panel shows movie of DIC images while the right panel shows time-lapse of ratio images (dye/FP). Magnification 40X; 2x2 binning. Movie acquired with 10 s interval. Time stamp on video indicates elapsed time; color bar indicates magnitude of ratio change. Src activation is seen at the cell edges.

Supplementary video 3: **Src activation in randomly migrating epithelial cells**. Time-lapse DIC (left panel) and ratio (right panel) images of the Src family merobody sensor in a randomly migrating Ptk1 epithelial cell is shown here. Magnification 60X; 2x2 binning. Movie acquired with 10 s interval. Time stamp on video indicates elapsed time; color bar indicates magnitude of ratio change. Several distinct regions of Src activation are seen including activation in cell protrusions.

Supplementary video 4: **Src activation at the cell edge and the effect of inhibitor**. Time-lapse DIC (left panel), sensor localization (middle panel) and ratio (right panel) images of the cell edge of a randomly protruding Ptk1 cell microinjected with merobody sensor. Also shown here is the effect of Src kinase inhibitor PP2, added to the cells at the indicated time point. Magnification 60X; 2x2 binning. Movie acquired with 10 s interval. Time stamp on video indicates elapsed time; color bar indicates magnitude of ratio change.

Supplementary video 5: **Merobody sensor is sensitive to Src activity**. Time-lapse DIC (left panel) and ratio (right panel) images of the Src family merobody sensor in a randomly migrating Ptk1 epithelial before and after addition of Src kinase inhibitor PP2. The timing of PP2 addition is highlighted in the time-lapse movies. Magnification 60X; 2x2 binning. Movie acquired with 10 s interval. Time stamp on video indicates elapsed time; color bar indicates magnitude of ratio change.

Supplementary video 6: **Src merobody sensor localization at the cell edge is dependent on Src activity**. Time lapse images of Src merobody sensor localization at the cell edge of a randomly protruding Ptk1 epithelial cell. Also shown is the effect of adding Src kinase inhibitor PP2 on sensor localization. PP2 causes sensor delocalization from the cell edge. Magnification 60X; 2x2 binning. Movie acquired with 10 s interval. Time stamp on video indicates elapsed time; color bar indicates magnitude of ratio change.

Supplementary Methods

Cell culture.

GN4 rat liver epithelial cells were grown in Richter's minimal essential medium supplemented with 10% heat-inactivated fetal bovine serum and penicillin/streptomycin/amphotericin B as described previously[2]. NIH 3T3 fibroblasts (MEFs) were cultured in 5% CO2 at 37°C in Dulbecco's modified Eagle's medium (DMEM, Mediatech) supplemented with 10 % fetal calf serum, 1 % L-Glutamine, and 1% penicillin streptomycin. PTK1 cells (ATCC CCL-35) were cultured in DMEM/F12 media (Gibco) supplemented with 8 % fetal calf serum, 1 % L-Glutamine, and 1% penicillin/streptomycin. MEFs and PTK1 cells were imaged in Ham's F-12K medium without phenol red (SAFC Biosciences) with 2% fetal bovine serum, 15mM HEPES, 1 % L-Glutamine, and 1% penicillin streptomycin.

Biosensor design and construct generation.

The biosensor construct was generated by overlapping PCR followed by restriction digestion and ligation into a modified pQE vector. The final biosensor construct has a 5' hexa-his tag, followed by NTs coding for mCerulean[3], a linker sequence and 1F11. See supplementary Figure 8 for the design and amino acid sequence of the biosensor. Various cysteine mutants as well as single proline point mutants were generated using the Quikchange (Stratagene) point mutagenesis kit starting with the mCerulean-linker-1F11 clone. Residue Alanine 24 of 1F11 was mutated to cysteine in the final biosensor construct. Non-binding versions of SFK merobody sensors were created by mutating proline 80 of 1F11 into alanine also using the Quikchange kit.

Protein expression and purification.

FN3 monobodies, including the binder 1F11 and wt FN3 (non-binding control) were expressed in E.coli BL21 (DE3) as described earlier[4]. The monobodies having a hexa-His tag were purified using Ni-affinity columns (His GraviTrap™) purchased from Amersham/GE healthcare as per manufacturer's instructions. A step gradient of imidazole was used in the elution of the proteins from the His GraviTrap™ columns to increase purity.

1F11-mCerulean fusion proteins were expressed in E.coli BL21 (DE3) as reported earlier[4]. Briefly, 1L cultures were induced with 1mM IPTG at RT for 14-16 hours before harvesting the bacteria. The biosensor fusion proteins with hexa-His tags were purified using Ni-affinity columns as described above. The proteins were examined for purity using SDS-PAGE.

Pulldown and in-vitro kinase experiments.

Cell Lysate Preparation: Prior to experiments, GN4 cells at 70–80% confluency were serum-starved overnight in Richter's minimum essential medium containing 0.1% fetal bovine serum. Following treatment as indicated, media was aspirated, and the cells were rinsed twice with ice-cold PBS. The cells were then scraped into ice-cold RIPA buffer (150 mM NaCl, 9.1 mM Na_2HPO_4, 1.7 mM NaH_2PO4, 1% Nonidet P-40, 0.5% sodium deoxycholate, and 0.1% SDS, pH 7.4) with freshly added 200 μM Na_3VO_4, 250 μM phenylmethylsulfonyl fluoride, 5 μg/ml leupeptin, and 10 nm microcysteine. The cell lysates were

clarified by centrifugation at 14,000 rpm for 10 min at 4 °C. Protein concentration of the supernatant was determined using the Coomassie protein assay reagent (Pierce).

Immunoblotting: In a typical experiment, 10 μg of cell lysate was resuspended in SDS-PAGE sample buffer (0.5 M Tris, pH 6.8, 4% SDS, 20% glycerol, 10% β-mercaptoethanol, 0.1% bromphenol blue) and heated at 95 °C for 5 min to denature proteins. The lysates were then resolved by SDS-PAGE on NuPAGE precast 10% Bis-Tris or NOVEX Tris-glycine gels (Invitrogen) and transferred to polyvinylidene fluoride (Immobilon-P; Millipore). The immunoblots were incubated with the appropriate primary antibody overnight at 4 °C, washed three times with TBST, and probed with horseradish peroxidase-conjugated secondary antibodies for 1 h at room temperature. Immunoblots were then developed with ECL (Amersham Biosciences) according to the manufacturer's instructions and visualized by autoradiography (Kodak X-Omat Blue film). For immunoblotting for total Src, antibodies B-12 and N-16 (Santa Cruz) were used.

Cell treatment: GN4 cells grown as described above were either left untreated before lysis, treated with vehicle (DMSO), or treated with a DMSO solution of Ciglitazone (Biomol), (±)-5-[4-(1-methylcyclohexylmethoxy)-benzyl]thiazolidine-2,4-dione, for either 10 or 30 minutes such that the final concentration of Ciglitazone was 50 μM. In order to inhibit phosphatases in a global manner, GN4 cells were pretreated with 50 μM pervanadate for 5 minutes.

Pull down assay: 200 μg of lysates (in RIPA buffer, no SDS) from GN4 cells, treated as described above, were incubated with 100 μg of either 1F11 or wt FN3 preabsorbed on 15 μL Ni sepharose (Qiagen) beads overnight with gentle agitation, in the presence of 20 mM Imidazole. The beads were washed once with RIPA (no SDS), thrice with ice cold PB and then resuspended in 20 μL Laemmeli buffer, boiled for 5 mintes, and subjected to SDS-PAGE, followed by analysis by western blots to look at total Src pulled-down by either the binder or control proteins.

In Vitro Src Kinase Assay: Src kinase activity in Src protein pulled down by either the binder (1F11) or wt FN3 from stimulated or unstimulated GN4 cells was measured using a commercial Src assay kit (Upstate Biotechnology, Inc.) according to the manufacturer's instructions. Briefly, Src was subjected to FN3 pull-down as described above from 200 μg of cell lysate by overnight incubation with either the binder or control. Src activity present in FN3-bead complexes was assessed by measuring the transfer of the γ-phosphate of [γ-^{32}P]ATP to a specific Src substrate peptide for 10 min at 30 °C. Phosphorylated substrate was then separated from residual [γ-^{32}P]ATP using P-81 phosphocellulose paper (Whatman) and quantified with a scintillation counter. The data reported here is an average of three independent experiments.

Dye labeling.

DMSO solutions of cysteine-reactive merocyanine dyes (10-20 mM) were added to 1F11-mCerulean fusion proteins (200-300 μM) in 50 mM HEPES, 100 mM NaCl buffer pH 7.4 such that the dye was present in 5-10 fold molar excess and the DMSO in the reaction mixture was less than 10%. After

reaction for 4-5 hours, excess dye was separated from labeled protein using size exclusion G-25 (GE healthcare) columns. During G-25 size exclusion, a clear separation was seen between the labeled protein band and the relatively immobile free dye. Labeled proteins were subjected to SDS-PAGE electrophoresis and a single fluorescent band was observed (controls in which labeled monobody and dye were mixed showed that free dye could be observed as a separate band of lower molecular weight). Coomassie labeling was also used to verify homogeneity of the biosensor preparations. Labeling efficiency was calculated by measuring the dye and protein concentrations of the labeled conjugate. Dye concentration was estimated using dye absorbance at absorption maxima after dissolving the conjugate in DMSO. Extinction coefficients have been reported elsewhere[5,6]. Protein concentration was estimated by using absorbance due to the mCerulean FP (molar extinction coefficient 43,000). Labeling efficiency was estimated to be in the range of 0.9-1.2 dye/protein molar ratio, for the various preparations tested. Binding to SH3 was compared for individual batches and similar results were obtained. Also, independent batches gave consistent results in live cell imaging experiments.

Binding assays.

The SH3 domain of c-Src was expressed, purified and analyzed as described earlier[4]. *In vitro* response of the biosensor was tested by recording fluorescence spectra of biosensor samples incubated with increasing concentrations of Src SH3 domain in PBS pH 7.4 at room temperature, using a SPEX fluorolog 3 spectrophotometer. Ratiometric response was measured by recording dye fluorescence (λ_{ex} 590 nm and λ_{em} 620 nm) as well as the mCerulean fluorescence (λ_{ex} 433 and λ_{ex} 477 nm). For estimation of binding constants, the average of three separate titrations was used. Each individual titration experiment consisted of samples measured in duplicate.

Microscopy.

For imaging experiments MEFs and PTK1 cells were plated onto coverslips coated with 5μg/mL Fibronectin (Sigma) overnight. Culture media was exchanged for imaging media for one hour prior to microinjection. Cells were microinjected using a biosensor concentration of 40μM in the microinjection needle, and were allowed to recover for 30-60min prior to imaging experiments. MEFs were stimulated using 30ng/mL PDGF (Sigma). For inhibiting SFKs PTK1 cells were treated with 10μM PP2 (Sigma).

Imaging was performed on an Olympus IX81 motorized inverted microscope equipped with ZDC focus drift compensator, a cooled digital 12-bit CCD camera (CoolSnap, Roper Scientific), a 100W Mercury arc lamp, and MetaMorph imaging software. Images were acquired using a 40X UPlanFLN 1.3 NA oil immersion objective (fibroblast cell experiments) or a 60X 1.2 NA UApo N Silicon oil immersion objective (PTK1 epithelial cells). A Multi-pass dichroic mirror (89006bs, Chroma) was used with the following band pass filters: m-Cerulean (ET 436/20, ET 480/40) and Mero-53 (HQ580/30, HQ 630/40). Images were acquired and processed as previously described[7,8].

Automated linescanning and analysis of Src activity

The response of the biosensor was analyzed using automated line scanning software. Line scans of length 100 pixels (~20 μm) were calculated at every pixel around the edge of the cell and oriented into the cell in a direction normal to the edge. The normal vector was calculated by making a binary image of the cell (pixels inside the cell equal one) and background, then applying a Gaussian filter to the image. This results in a gradient from zero to one across the cell edge. A contour line (of equal intensities) around the cell edge was taken a smooth approximation to the pixilated edge. From this a smooth normal vector was calculated. The normal vector at a pixel on the edge of the cell was taken to be the nearest normal vector on the contour. Intensities along the scanning line were bi-linearly interpolated from the four neighboring pixels.

Velocity of the cell boundary in between subsequent images was calculated by a mechanical model similar to that described previously[9]. However, we altered this model to include $1/r^2$ repulsion terms between marker points on the boundary in order to avoid topological violations.

Each linescan originates at a pixel at the cell edge, and for each pixel we calculated a velocity from the mechanical model. Linescans were then grouped by velocity into bins of width 0.0022 μm s^{-1}. As a result of this analysis we stored a matrix indexed by velocity in one dimension and linescan depth in the other. We also stored the number of pixels in each velocity bin.

Nine Ptk1 cells were analyzed in this fashion. The results were averaged by a weighted mean (by the number of pixels in each bin) of the nine velocity-linescan matrices. Five of the nine cells were treated with PP2 at a given time-point. Unless otherwise noted, the data from before PP2 treatment was used. The post-PP2 data was compared with pre-PP2 treatment in the same cells, so n=5 in this analysis. For the standard error see legend to main text **Fig. 5a**. The difference between the intensity ratios before and after PP2 addition at 1μm was significance tested using a t-test with equal variance and unequal sample sizes. Before PP2 treatment n=119,721 and for after n=135,511, and the standard deviation in both cases was ~0.12.

Modeling of dye on 1F11/SH3 interface

Structure models were generated with the AnchoredDesign package within the Rosetta3 series of software [10]. This package was designed to model docked structures mediated by flexible surface loops, especially where there was evidence for a particular binding mode. In this case, the polyproline motif in 1F11 was aligned to a sequence-matched polyproline motif in PDB structure 1QWF, which contains a peptide bound to a cSrc SH3 domain [11,12]. Starting from this structure, and holding the polyproline region constant, the surface loops of the monobody (including the regions mutated by Karatan et al[4] were remodeled and minimized and the sidechains repacked. Conformations for the dye molecule were pregenerated as a rotamer library, also using the Rosetta3 software; thus conformational sampling for the dye proceeded simultaneously with normal sidechain packing (details to be reported elsewhere).

Unbound models were produced in the same fashion, except that the cSrc-SH3 domain was not present as a docking partner and the polyproline motif was not held constant.

Approximately 6000-7000 structures were produced for each bound model (positions 24, 53, and 55), and approximately twice as many for the unbound models. This represents approximately 1024 processor-days on a 2.3 GHz processor per group of models.

The models were analyzed by calculating the per-atom solvent accessible surface area, again using the Rosetta software package. SASA was calculated for the entire dye residue (the fluorophore, the linker, and the cysteine backbone within the protein), the fluorophore region, the SO_3 group, the carbonyl group, and the sulfone group. Generally the SO_3 and carbonyl distributions were uninformative. The whole-residue SASA contains a great deal of noise from fluorescence-irrelevant atoms. The fluorophore and sulfone distributions are reported here for all 6 combinations of dye position and binding.

References

1. Dewar, B.J. et al. Capacitative calcium entry contributes to the differential transactivation of the epidermal growth factor receptor in response to thiazolidinediones. *Mol Pharmacol* **72**, 1146-56 (2007).
2. Gardner, O.S., Dewar, B.J., Earp, H.S., Samet, J.M. & Graves, L.M. Dependence of peroxisome proliferator-activated receptor ligand-induced mitogen-activated protein kinase signaling on epidermal growth factor receptor transactivation. *J Biol Chem* **278**, 46261-9 (2003).
3. Rizzo, M.A., Springer, G.H., Granada, B. & Piston, D.W. An improved cyan fluorescent protein variant useful for FRET. *Nat Biotechnol* **22**, 445-9 (2004).
4. Karatan, E. et al. Molecular recognition properties of FN3 monobodies that bind the Src SH3 domain. *Chem Biol* **11**, 835-44 (2004).
5. Toutchkine, A., Kraynov, V. & Hahn, K. Solvent-sensitive dyes to report protein conformational changes in living cells. *J Am Chem Soc* **125**, 4132-45 (2003).
6. Toutchkine, A., Nguyen, D.V. & Hahn, K.M. Simple one-pot preparation of water-soluble, cysteine-reactive cyanine and merocyanine dyes for biological imaging. *Bioconjug Chem* **18**, 1344-8 (2007).
7. Hodgson, L., Nalbant, P., Shen, F. & Hahn, K. Imaging and photobleach correction of Mero-CBD, sensor of endogenous Cdc42 activation. *Methods Enzymol* **406**, 140-56 (2006).
8. Hodgson, L., Shen, F. & Hahn, K. Biosensors for characterizing the dynamics of rho family GTPases in living cells. *Curr Protoc Cell Biol* **Chapter 14**, Unit 14 11 1-26.
9. Machacek, M. & Danuser, G. Morphodynamic profiling of protrusion phenotypes. *Biophys J* **90**, 1439-52 (2006).
10. Das, R. & Baker, D. Macromolecular modeling with rosetta. *Annu Rev Biochem* **77**, 363-82 (2008).
11. Feng, S., Kasahara, C., Rickles, R.J. & Schreiber, S.L. Specific interactions outside the proline-rich core of two classes of Src homology 3 ligands. *Proc Natl Acad Sci U S A* **92**, 12408-15 (1995).
12. Berman, H.M. et al. The Protein Data Bank. *Nucleic Acids Res* **28**, 235-42 (2000).